AIMS Mathematics, 8(5): 12559–12575.
DOI: 10.3934/math.2023631
Received: 18 October 2022
Revised: 17 November 2022
Accepted: 18 December 2022
Published: 27 March 2023

http://www.aimspress.com/journal/Math

Research article

Numerical investigations of nonlinear Maxwell fluid flow in the presence of non-Fourier heat flux theory: Keller box-based simulations

Afraz Hussain Majeed[1,†], Sadia Irshad[2], Bagh Ali[3], Ahmed Kadhim Hussein[4,5], Nehad Ali Shah[6,†] and Thongchai Botmart[7,*]

[1] Department of Mathematics, Air University, PAF Complex E-9, Islamabad 44000, Pakistan
[2] Institute of Mathematics, Khwaja Fareed University of Engineering and Information Technology, Rahim Yar Khan, Punjab 64200, Pakistan
[3] Faculty of Computer Science and Information Technology, Superior University, Lahore 54000, Pakistan
[4] Mechanical Engineering Department, College of Engineering, University of Babylon, Hilla 00964, Iraq
[5] College of Engineering, University of Warith Al-Anbiyaa, Karbala 56001, Iraq
[6] Department of Mechanical Engineering, Sejong University, Seoul 05006, South Korea
[7] Department of Mathematics, Faculty of Science, Khon Kaen University, Khon Kaen 40002, Thailand

[*]**Correspondence author:** Email: thongbo@kku.ac.th.

† These authors contributed equally to this work and are co-first authors.

Abstract: We investigate the thermal flow of Maxwell fluid in a rotating frame using a numerical approach. The fluid has been considered a temperature-dependent thermal conductivity. A non-Fourier heat flux term that accurately reflects the effects of thermal relaxation is incorporated into the model that is used to simulate the heat transfer process. In order to simplify the governing system of partial differential equations, boundary layer approximations are used. These approximations are then transformed into forms that are self-similar with the help of similarity transformations. The mathematical model includes notable quantities such as the rotation parameter λ, Deborah number β, Prandtl number Pr, parameter ϵ and the dimensionless thermal relaxation times γ. These are approximately uniformly convergent. The Keller box method is used to find approximate solutions to ODEs. We observed due to the addition of elastic factors, the hydrodynamic boundary layer gets

thinner. The thickness of the boundary layer can be reduced with the use of the k rotation parameter as well. When *Pr* increases, the wall slope of the temperature increases as well and approaches zero, which is an indication that *Pr* is decreasing. In addition, a comparison of the Cattaneo-Christov (CC) and Fourier models are provided and discussed.

Keywords: Maxwell fluid; CC model; rotating surface; heat flux; Keller box method
Mathematics Subject Classification: 76-10, 76R10

1. Introduction

Generalized Newtonian fluid mechanics has been a inspirational field as it describes such central problems from food processing, chemical and petroleum industries. Its models are valuable to find the effects of fluid flow in nature and industries such as biological fluid, pastes, polymeric liquids and numerous complicated mixtures. Viscoelastic fluids are exclusive generalized Newtonian fluids in which the shear-stress memory function of deformation rate. In these types of fluids, the deformation rate generally decreases when the shear stress is eliminated. This phenomenon is called stress relaxation. Many researchers have given special concentrate to the boundary layer flows of Maxwell fluid in the current background. The coupled flow and heat transfer of an upper-convected Maxwell fluid over a stretching plate with a velocity slip barrier was investigated by Han et al. [1]. The work under consideration obtained an analytical solution. The rotating flow of upper-convected Maxwell fluid was studied using the CC heat flux model by Mustafa [2], and it was discovered that the fluid velocity significantly rises. Bhattacharyya et al. [3] have introduced multiple results for Maxwell fluid with a porous shrinking surface by shooting numerical scheme. Fetecau et al. [4,5] have introduced the unsteady flows in Maxwell fluid with oscillation and acceleration mature in the rigid body in flow. Mahsud et al. [6] studied the Influence of time-fractional derivatives on the boundary layer flow of Maxwell fluids. It introduced that the Maxwell fluid is reasonable for relaxation effects which can't be forecast in other various kinds of non-Newtonian fluid. Khan et al. [7] give a scientific report on heat transfer analysis in mixed convection flow of Maxwell fluid over an oscillating vertical plate. S. K. Nandy [8] investigated the heat transfer assessment over a decreasing sheet with the Navier slip effect and unsteady upper-convected Maxwell nanofluid flow, and they found that the quantities of the Nusselt number increased with increasing values of the Maxwell variable. Shah et al. [9] provided an idea of Maxwell fluid flow between vertical plates with damped shear and thermal flux a free convection phenomenon. Cao et al. [10] investigated the steady flow of Maxwell fluid over a porous medium using an interpolation methodology that is equivalent to the implicit RK. scheme. The expanding subject of engineering known as hybrid nano-liquid has captured the attention of a large number of researchers who were seeking for ways to increase the efficiency of cooling processes used in industry. These researchers were looking for ways to improve the effectiveness of cooling processes. A nano-liquid is a type of fluid that is created when powerful particles with sizes less than 100 nm in diameter are propagated in other fluids. One of the noticeable properties of a nano-liquid is its low thermal conductivity, which is one of the characteristics that can hinder the effectiveness of heat transport. Karim and Samad [11] examined the effect of Brownian diffusion with CC heat flux on viscoelastic squeeze nanofluid flow and double slip impact in a channel. Specifically, they focused on the effects of these two factors. The effect of thermal radiation on the transmission of heat and mass through an unstable stretched surface

was examined by Shateyi and Motsa [12]. Additionally, they noticed that when the values of the unsteadiness parameter grew, the velocity profiles and concentration distributions decreased. Abel et al. [13] used a numerical approximation to study the flow of a Maxwell material close to a stretchy surface. The temperature of the fluid medium above the sheet decreases when the radiation parameter is increased. When necessary, this effect might be employed to quicken the sheet's cooling process. The Maxwell effect's implications in relation to issues with molecular transport were examined by C. I. Christov [14]. To the best of authors' knowledge, no attempt has yet been made to include the Maxwell delay in the closure models for turbulent fluxes, and this potential is explored in the current study. B. Straughan [15] used a Cattaneo-type constitutive energy equation to investigate the heat flux caused by thermal convection in an incompressible viscous fluid. They showed that when the Cattaneo number is high enough and the convection mechanism flips from stationary convection to oscillatory convection for smaller magnitudes, thermal relaxation exhibits a significant influence. Tibullo et al. [16] introduced the uniqueness of solutions for heat transfer in an incompressible fluid by Cattaneo-Shristov law. In the framework of the CC model, S. Hadded [17] analyzes the thermal instability of flow through a porous media.

Aims of this paper are the numerical study of viscoelastic fluid flow in rotating surfaces with variable thermal conductivity. In this, firstly, mathematical modeling for laminar flow of Maxwell fluid with a stretchable rotating surface. Secondly, to investigate the effects of heat transfer with thermal conductivity. Finally, to solve numerical results by using the Keller box based on a finite difference scheme. Furthermore, the following strategy is being utilized for the current communication: The equation that describes the characteristics of fluid flow can be found in Section 2 of the document. Section 3 disclosure includes the procedure for the numerical system that was implemented. In Section 4, the primary conclusions are presented in the form of rough sketches of a few of the involved quantities. In Section 5, the results are discussed.

2. Mathematical modeling

Let's imagine a stretchy surface as an incompressible Maxwell fluid laminar flow (see Figure 1).

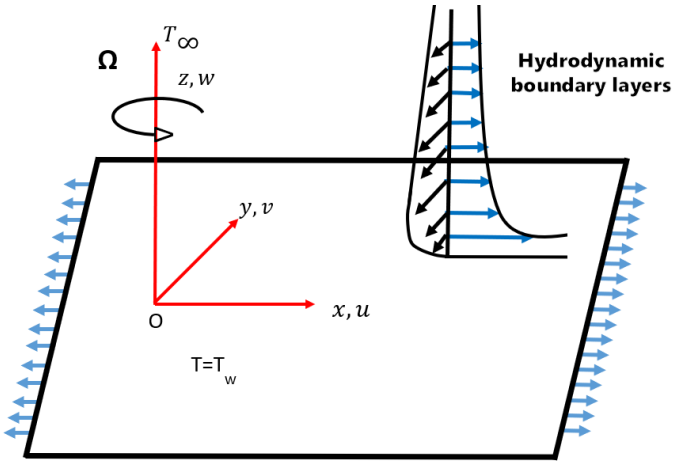

Figure 1. Schematic diagram of the problem.

We choose the Cartesian coordinate system so that the fluid is taken into account in space $z \geq 0$ and the surface is aligned with the xy-plane. The fluid is considered to spin continuously about the z-axis with constant angular velocity Ω while the surface is assumed to stretch in the x-direction at a greater rate. We investigate a non-Fourier heat conduction model because the temperature of the sheet, denoted by the symbol T_W, is constant and is thought to be higher than the ambient temperature T_∞.

Below are given the pertinent equations that represent the Maxwell fluid flow in a rotating frame [6].

$$\nabla.\mathbf{V} = \mathbf{0}, \tag{2.1}$$

$$\{(\boldsymbol{V}.\nabla)\boldsymbol{V} + (\boldsymbol{\Omega} \times (\boldsymbol{\Omega} \times \boldsymbol{r})) + (2\boldsymbol{\Omega} \times \boldsymbol{V})\} = -\nabla p + \nabla.\boldsymbol{S}, \tag{2.2}$$

where the pressure and fluid density are denoted by p and ρ, while the angular velocity is $\boldsymbol{\Omega} = [0, 0, \Omega]$. The stress tensor **S** for upper-convected Maxwell fluid follows the relation

$$\left(1 + \lambda_1 \frac{D}{Dt}\right)\boldsymbol{S} = \mu \mathbf{A}_1, \tag{2.3}$$

where the fluid relaxation time is λ_1, first Rivlin-Ericksen tensor is $\mathbf{A}_1 = (\nabla \boldsymbol{V}) + (\nabla \boldsymbol{V})^T$ and the derivative of upper-convection with time is $\frac{D}{Dt}$. For second rank tensor **S** and vector **a,** as

$$\frac{D\boldsymbol{S}}{Dt} = \frac{\partial \boldsymbol{S}}{\partial t} + (\mathbf{V}.\nabla)\boldsymbol{S} - \boldsymbol{L}\boldsymbol{S} - \boldsymbol{S}\boldsymbol{L}^{\boldsymbol{T}}, \tag{2.4}$$

$$\frac{D\boldsymbol{a}}{Dt} = \frac{\partial \boldsymbol{a}}{\partial t} + (\mathbf{V}.\nabla)\boldsymbol{a} - \boldsymbol{L}\boldsymbol{a}, \tag{2.5}$$

Now, consider $\left(1 + \lambda_1 \frac{D}{Dt}\right)$ operator to applying in Eq (2.3), then compute the component forms after implementation of boundary layer approximation while the resulting equations are obtained as [18]

$$\mathrm{u}\frac{\partial u}{\partial x} + v\frac{\partial u}{\partial y} + w\frac{\partial u}{\partial z} - 2\Omega v + \lambda_1 \left[\begin{array}{l} u^2\frac{\partial^2 u}{\partial x^2} + v^2\frac{\partial^2 u}{\partial y^2} + w^2\frac{\partial^2 u}{\partial z^2} + 2uv\frac{\partial^2 u}{\partial x \partial y} + 2vw\frac{\partial^2 u}{\partial y \partial z} \\ +2uw\frac{\partial^2 u}{\partial x \partial z} - 2\Omega\left(u\frac{\partial v}{\partial x} + v\frac{\partial v}{\partial y} + w\frac{\partial v}{\partial z}\right) \\ +2\Omega\left(v\frac{\partial u}{\partial x} - u\frac{\partial u}{\partial y}\right) \end{array}\right] = \nu\frac{\partial^2 u}{\partial z^2}, \tag{2.6}$$

$$\mathrm{u}\frac{\partial v}{\partial x} + v\frac{\partial u}{\partial y} + w\frac{\partial v}{\partial z} + 2\Omega u + \lambda_1 \left[\begin{array}{l} u^2\frac{\partial^2 u}{\partial x^2} + v^2\frac{\partial^2 u}{\partial y^2} + w^2\frac{\partial^2 u}{\partial z^2} + 2uv\frac{\partial^2 u}{\partial x \partial y} + 2vw\frac{\partial^2 u}{\partial y \partial z} \\ +2uw\frac{\partial^2 u}{\partial x \partial z} + 2\Omega\left(u\frac{\partial v}{\partial x} + v\frac{\partial v}{\partial y} + w\frac{\partial v}{\partial z}\right) \\ +2\Omega\left(v\frac{\partial u}{\partial x} - u\frac{\partial u}{\partial y}\right) \end{array}\right] = \nu\frac{\partial^2 v}{\partial z^2}, \tag{2.7}$$

The energy balance equation is provided by under the supposition that viscous dissipation and heat generation/absorption effects are zero.

$$\rho c_p(\mathbf{V}\cdot\nabla T) = -\nabla\cdot\mathbf{q}, \tag{2.8}$$

$$\mathbf{q} = -\lambda_3\left(\frac{\partial \mathbf{q}}{\partial t} + \mathbf{V}\cdot\nabla\mathbf{q} - \mathbf{q}\cdot\nabla\mathbf{V} + (\nabla\cdot\mathbf{V})\mathbf{q}\right) - k\nabla T, \tag{2.9}$$

where k is the thermal conductivity and λ_3 is the thermal relaxation time. The time delay required for the start of a heat flow after a temperature gradient has been introduced at a certain place is known as the thermal relaxation time. The heat can be transported via thermal waves that travel at a finite rate according to the non-Fourier heat flux phenomenon. We eliminate **q** from Eqs (2.8) and (2.9) to achieve the following:

$$\begin{aligned} &\mathrm{u}\frac{\partial T}{\partial x} + v\frac{\partial u}{\partial y} + w\frac{\partial T}{\partial z} \\ &= \frac{1}{\rho c_p}\frac{\partial}{\partial z}\left(k\frac{\partial T}{\partial z}\right) - \lambda_3\left(\begin{array}{l} u^2\frac{\partial^2 u}{\partial x^2} + v^2\frac{\partial^2 u}{\partial y^2} + w^2\frac{\partial^2 u}{\partial z^2} + 2uv\frac{\partial^2 u}{\partial x\partial y} + 2vw\frac{\partial^2 u}{\partial y\partial z} + \\ 2uw\frac{\partial^2 u}{\partial x\partial z} + \left(u\frac{\partial v}{\partial x} + v\frac{\partial v}{\partial y} + w\frac{\partial v}{\partial z}\right) + \left(v\frac{\partial u}{\partial x} - u\frac{\partial u}{\partial y}\right) \end{array}\right). \end{aligned} \tag{2.10}$$

The flow is subjected to the following conditions:

$$\begin{cases} u = ax,\ v = 0,\ w = o,\ T = T_w, & \text{at } z = 0, \\ u \to 0,\ v \to 0,\ T \to T_\infty, & \text{at } z \to \infty. \end{cases} \tag{2.11}$$

We seek the similarity solution of the problem in the following form:

$$f'(\eta) = \frac{u}{ax},\ g(\eta) = \frac{v}{ax},\ \mathrm{w} = -\sqrt{av}\,f(\eta),\ \theta(T_w - T_\infty) = (T - T_\infty),\ \eta = \sqrt{\frac{a}{v}}z, \tag{2.12}$$

where prime denotes a change in differentiation with regard to η. The equation $k = k_\infty\left[1 + \frac{\epsilon(T-T_\infty)}{\Delta T}\right]$, where $\epsilon > 0$ is a positive constant and k_∞ specifies the thermal conductivity at ambient temperature, further assumes that the thermal conductivity varies with temperature T. Equation (2.1) is automatically satisfied by transformation (2.12), and Eqs (2.6), (2.7) and (2.10) are transformed into the following differential equations:

$$f''' + ff'' - f'^2 + 2\lambda g - 2\lambda\beta fg' + 2\beta ff'f'' - \beta f^2 f''' = 0, \tag{2.13}$$

$$g'' + fg' - f'g - 2\lambda f' - 2\lambda\beta\left(f'^2 - ff'' + g^2\right) + \beta\left(2ff'g' - f^2 g''\right) = 0, \tag{2.14}$$

$$\left[1 + \in\theta\right]\theta'' + \in\theta'^2 + Prf\theta' - \gamma Pr\left[ff'\theta' + f^2\theta''\right] = 0, \tag{2.15}$$

assuming to the transformed conditions:

$$\begin{cases} f=0,\ g=0,\ f'=1,\ \theta=1, & \text{at } \eta\to 0, \\ f'\to 0,\ g\to 0,\ \theta\to 0, & \text{at } \eta\to\infty, \end{cases} \tag{2.16}$$

where $\beta=\lambda_1 a$ is relaxation time, $\gamma=\lambda_3 a$ is thermal relaxation, $Pr={}^{\mu c_p}/_{k}$ is the Prandtl number, $\lambda={}^{\Omega}/_{a}$ is the Ratio of rotation and stretching rates.

3. Numerical approach

The physical perception of the current work requires the manipulation of an accurate solution. Karman approximation is used to model the equations at first, and then we arrive at the nonlinear system of ordinary differential equations (2.13)–(2.15) along with boundary conditions in Eq (2.16). Therefore, we used the implicit finite difference Keller-box approach that is mentioned in [19–21]. As follows are the details of the Keller Box Method:

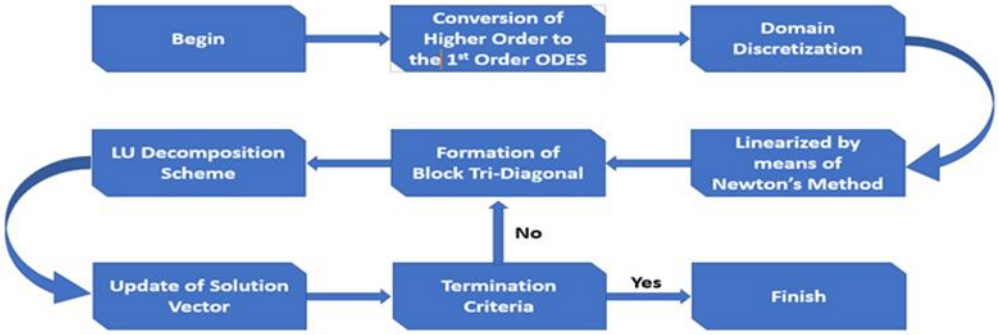

Figure 2. Keller box method.

In order to use this strategy, we must first convert to a system of first-order equations and establish new variables $u(z,\eta)$, $v(z,\eta)$, $g(z,\eta)$, $w(z,\eta)$, $p(z,\eta)$ and $\theta(z,\eta)$ are

$$f'=u,\ u'=v,\ g'=w,\ \theta'=p, \tag{3.1}$$

$$v'+fv-u^2+2\lambda(g-\beta+w)+\beta(2fuv-f^2v')=0, \tag{3.2}$$

$$w'+fw-ug-2\lambda(u+\beta[u^2-fv+g^2])+\beta(2fuv-f^2w')=0, \tag{3.3}$$

$$(1+\epsilon\theta)p'+P_r fp-P_r\gamma(fup+f^2p')=0, \tag{3.4}$$

Implementing the Newton iteration $f_{j+1}=f_j+\delta f_j$ for all dependent variables included in the linearized nonlinear algebraic equations, substituting these formulations in the differential systems, and ignoring quadratic and higher order terms in δ the following linear tridiagonal arrangement:

$$\delta f_j-\delta f_{j-1}-\frac{1}{2}h\left(\delta u_j+\delta u_{j-1}\right)=(r_1)_{j-\frac{1}{2}},$$

$$\delta u_j-\delta u_{j-1}-\frac{1}{2}h\left(\delta v_j+\delta v_{j-1}\right)=(r_2)_{j-\frac{1}{2}},$$

$$\delta g_j - \delta g_{j-1} - \frac{1}{2}h\left(\delta w_j + \delta w_{j-1}\right) = (r_3)_{j-\frac{1}{2}},$$

$$\delta \theta_j - \delta \theta_{j-1} - \frac{1}{2}h\left(\delta p_j + \delta p_{j-1}\right) = (r_4)_{j-\frac{1}{2}},$$

where

$$f_{j-1} - f_j + \frac{h}{2}\left(u_j + u_{j-1}\right) = (r_1)_{j-\frac{1}{2}},$$

$$u_{j-1} - u_j + \frac{h}{2}\left(v_j + v_{j-1}\right) = (r_2)_{j-\frac{1}{2}},$$

$$g_{j-1} - g_j + \frac{h}{2}\left(w_j + w_{j-1}\right) = (r_3)_{j-\frac{1}{2}},$$

$$\theta_{j-1} - \theta_j + \frac{h}{2}\left(p_j + p_{j-1}\right) = (r_4)_{j-\frac{1}{2}},$$

$$\psi_1 = \psi_2 = \frac{1}{4}\left(v_j + v_{j-1}\right) - \frac{\lambda\beta h}{2}\left(w_j + w_{j-1}\right) + \frac{\beta h}{4}\left(u_j + u_{j-1}\right)\left(v_j + v_{j-1}\right)$$
$$-\frac{\beta}{2}\left(f_j + f_{j-1}\right)\left(v_j + v_{j-1}\right),$$

$$\psi_3 = \psi_4 = -\frac{h}{2}\left(u_j + u_{j-1}\right) + \frac{\beta h}{4}\left(v_j + v_{j-1}\right)\left(f_j + f_{j-1}\right),$$

$$\psi_5 = 1 + \frac{h}{4}\left(f_j + f_{j-1}\right) + \frac{\beta h}{4}\left(u + u_{j-1}\right)\left(f_j + f_{j-1}\right) - \frac{\beta}{4}\left(f_j + f_{j-1}\right)^2,$$

$$\psi_6 = -1 + \frac{h}{4}\left(f_j + f_{j-1}\right) + \frac{\beta h}{4}\left(u + u_{j-1}\right)\left(f_j + f_{j-1}\right) - \frac{\beta}{4}\left(f_j + f_{j-1}\right)^2,$$

$$\psi_7 = \psi_8 = \lambda h,$$

$$\psi_9 = \psi_{10} = \frac{\lambda h}{2}\left(f_i + f_{j-1}\right).$$

Also,

$$(r_5)_{j+\frac{1}{2}} = v_{j+1} - v_j - \frac{h}{4}\left(f_j + f_{j-1}\right)\left(v_j + v_{j-1}\right) + \frac{h}{4}\left(v_j + v_{j-1}\right)^2$$
$$-h\lambda\left(g_j - g_{j-1}\right) + \frac{h\beta_1}{2}\left(f_j + f_{j-1}\right)\left(v_j + v_{j-2}\right),$$

$$\alpha_1\delta f_j + \alpha_2\delta f_{j-1} + \alpha_3\delta u_j + \alpha_4\delta u_{j-1} + \alpha_5\delta v_j + \alpha_6\delta v_{j-1}$$
$$+\alpha_7\delta g_j + \alpha_8\delta g_{j-1} + \alpha_9\delta w_j + +\alpha_{10}\delta g_{j-1} = (r_6)_{j-1},$$

$$\alpha_1 = \alpha_2 = \frac{h}{4}(w_j + w_{j-1}) + \frac{\lambda\beta h}{2}(v_j + v_{j-1}) - \frac{\beta h}{4}(u_j + u_{j-1})(w_j + w_{j-1}) - \frac{\beta}{2}(f_j + f_{j-1})(w_j + w_{j-1}),$$

$$\alpha_3 = \alpha_4 = \frac{\beta h}{4}(f_j + f_{j-1})(w_j + w_{j-1}) - \frac{h}{4}(g_j + g_{j-1}) - \lambda h - \lambda\beta h(f_j + f_{j-1})(u_j + u_{j-1}),$$

$$\alpha_5 = \alpha_6 = \frac{\lambda\beta h}{2}(f_j + f_{j-1}),$$

$$\alpha_7 = \alpha_8 = -\frac{h}{4}(u_j + u_{j-1}) - 2h\lambda\beta(g_j + g_{j-1}),$$

$$\alpha_9 = 1 + \frac{h}{4}(f_j + f_{j-1}) + \frac{\beta h}{4}(f_j + f_{j-1})(u_j + u_{j-1}) - \frac{\beta}{4}(f_j + f_{j-1})^2,$$

$$\alpha_{10} = -1 + \frac{h}{4}(f_j + f_{j-1}) + \frac{\beta h}{4}(f_j + f_{j-1})(u_j + u_{j-1}) - \frac{\beta}{4}(f_j + f_{j-1})^2.$$

Also,

$$(r_6)_{j-1} = w_{j-1} - w_j - \frac{h}{4}(f_j + f_{j-1})(w_j + w_{j-1}) + \frac{h}{4}(f_j + f_{j-1})(g_j + g_{j-1}) + 2h\lambda\left(\frac{u_j - u_{j-1}}{2}\right) + \beta\left[\left(\frac{u_j - u_{j-1}}{2}\right)^2 - \left(\frac{f_j - f_{j-1}}{2}\right)\left(\frac{v_j - v_{j-1}}{2}\right) + \left(\frac{g_j - g_{j-1}}{2}\right)^2\right] - \beta h\left[2\left(\frac{f_j - f_{j-1}}{2}\right)\left(\frac{u_j - u_{j-1}}{2}\right)\left(\frac{w_j - w_{j-1}}{2}\right) - \left(\frac{f_j - f_{j-1}}{2}\right)^2\left(\frac{w_j - w_{j-1}}{h}\right)\right],$$

$$\beta_1\delta f_j + \beta_2\delta f_{j-1} + \beta_3\delta u_j + \beta_4\delta u_{j-1} + \beta_5\delta\theta_j + \beta_6\delta\theta_{j-1} + \beta_7\delta p_j + \beta_8\delta p_8 = (r_7)_{j-1},$$

$$\beta_1 = \beta_2 = \frac{P_r h}{4_{j_{j-1}}\frac{P_r rh}{\theta}(u_j + {}_{j-1})\frac{P_r r}{2}(f_j + {}_{j-1})},$$

$$\beta_3 = \beta_4 = -\frac{P_r rh}{8}(f_j + f_{j-1})(p_j + p_{j-1}),$$

$$\beta_5 = \beta_6 = \varepsilon(p_j - p_{j-1}),$$

$$\beta_7 = (1 + \varepsilon\theta) + \frac{\varepsilon h}{2}(p_j + p_{j-1}) + \frac{P_r h}{4 f_j + {}_{j-1}\frac{P_r rh}{8}u_j + {}_{j-1} f_j + {}_{j-1}\frac{P_r r}{4} f_j + {}_{j-1}{}^2},$$

$$\beta_8 = -(1 + \varepsilon\theta) + \frac{\varepsilon h}{2}(p_j + p_{j-1}) + \frac{P_r h}{4 f_j + {}_{j-1}\frac{P_r rh}{8}u_j + {}_{j-1} f_j + {}_{j-1}\frac{P_r r}{4} f_j - {}_{j-1}{}^2},$$

$$(r_7)_{j-\frac{1}{2}} = \left(1 + \varepsilon\left(\frac{\theta_j + \theta_{j-1}}{2}\right)\right)(p_{j-1} - p_j) - \varepsilon h\left(\frac{p_j + p_{j-1}}{2}\right)^2 - P_r h\left(\frac{f_j + f_{j-1}}{2}\right)\left(\frac{p_j + p_{j-1}}{2}\right) + P_r\, r\, h\left[\left(\frac{f_j + f_{j-1}}{2}\right)\left(\frac{u_j + u_{j-1}}{2}\right)\left(\frac{p_j + p_{j-1}}{2}\right) + \left(\frac{f_j + f_{j-1}}{2}\right)^2\left(\frac{p_j + p_{j-1}}{h}\right)\right].$$

The block tridiagonal structure of the linearized difference equation often consists of variables or constants, but in this case, it consists of block matrices. The matrix elements in our scenario are defined as follows:

$$\begin{bmatrix} [\mathbf{A_1}] & [\mathbf{C_2}] & \cdot & \cdot & \cdot & \cdot \\ [\mathbf{B_2}] & [\mathbf{A_2}] & [\mathbf{C_2}] & \cdot & \cdot & \cdot \\ \cdot & \cdot & \cdot & \cdot & \cdot & \cdot \\ \cdot & \cdot & \cdot & \cdot & \cdot & \cdot \\ \cdot & \cdot & \cdot & \cdot & \cdot & \cdot \\ \cdot & \cdot & \cdot & [\mathbf{B_{j-1}}] & [\mathbf{A_{j-1}}] & [\mathbf{C_{j-1}}] \\ \cdot & \cdot & \cdot & \cdot & [\mathbf{B_j}] & [\mathbf{A_j}] \end{bmatrix} \begin{bmatrix} [\delta_1] \\ [\delta_2] \\ \cdot \\ \cdot \\ \cdot \\ [\delta_{j-1}] \\ [\delta_j] \end{bmatrix} = \begin{bmatrix} [r_1] \\ [r_2] \\ \cdot \\ \cdot \\ \cdot \\ [r_{j-1}] \\ [r_j] \end{bmatrix}.$$

That is $[A][\delta] = [r]$, where

$$A_1 = \begin{bmatrix} 1 & 0 & 0 & 0 & 0 & 0 & 0 \\ 0 & 1 & 0 & 0 & 0 & 0 & 0 \\ 0 & 0 & 0 & 1 & 0 & 0 & 0 \\ 0 & 0 & 0 & 0 & 0 & 1 & 0 \\ 0 & 1 & \frac{-h}{2} & 0 & 0 & 0 & 0 \\ 0 & 0 & 0 & 1 & \frac{-h}{2} & 0 & 0 \\ 0 & 0 & 0 & 0 & 0 & 1 & \frac{-h}{2} \end{bmatrix},$$

$$B_2 = \begin{bmatrix} 1 & \frac{-h}{2} & 0 & 0 & 0 & 0 & 0 \\ \Psi_1 & \Psi_3 & \Psi_5 & \Psi_7 & \Psi_9 & 0 & 0 \\ \alpha_1 & \alpha_3 & \alpha_5 & \alpha_7 & \alpha_9 & 0 & 0 \\ \beta_1 & \beta_3 & 0 & 0 & 0 & \beta_5 & \beta_7 \\ 0 & 0 & 0 & 0 & 0 & 0 & 0 \\ 0 & 0 & 0 & 0 & 0 & 0 & 0 \\ 0 & 0 & 0 & 0 & 0 & 0 & 0 \end{bmatrix},$$

$$C2 = \begin{bmatrix} 0 & 0 & 0 & 0 & 0 & 0 & 0 \\ 0 & 0 & 0 & 0 & 0 & 0 & 0 \\ 0 & 0 & 0 & 0 & 0 & 0 & 0 \\ 0 & 0 & 0 & 0 & 0 & 0 & 0 \\ 0 & -1 & \frac{-h}{2} & 0 & 0 & 0 & 0 \\ 0 & 0 & 0 & -1 & \frac{-h}{2} & 0 & 0 \\ 0 & 0 & 0 & 0 & 0 & -1 & \frac{-h}{2} \end{bmatrix},$$

$$A_2=\begin{bmatrix} -1 & \frac{-h}{2} & 0 & 0 & 0 & 0 & 0 \\ \Psi_1 & \Psi_4 & \Psi_6 & \Psi_8 & \Psi & 0 & 0 \\ \alpha_2 & \alpha_1 & \alpha_6 & \alpha_8 & \alpha_{10} & 0 & 0 \\ \beta_2 & \beta_4 & 0 & 0 & 0 & \beta_6 & \beta_8 \\ 0 & 1 & \frac{-h}{2} & 0 & 0 & 0 & 0 \\ 0 & 0 & 0 & -1 & \frac{-h}{2} & 0 & 0 \\ 0 & 0 & 0 & 0 & 0 & 1 & \frac{h}{2} \end{bmatrix}.$$

We assume that A is nonsingular and it can be factored into $[A]=[L][U]$, where

$$[L]=\begin{bmatrix} [\boldsymbol{\alpha_1}] & \cdot & \cdot & \cdot & \cdot & \cdot \\ [\boldsymbol{\beta_2}] & [\boldsymbol{\alpha_2}] & \cdot & \cdot & \cdot & \cdot \\ \cdot & \cdot & \cdot & \cdot & \cdot & \cdot \\ \cdot & \cdot & \cdot & \cdot & \cdot & \cdot \\ \cdot & \cdot & \cdot & \cdot & \cdot & \cdot \\ \cdot & \cdot & \cdot & \cdot & [\boldsymbol{\alpha_{j-1}}] & \cdot \\ \cdot & \cdot & \cdot & \cdot & [\boldsymbol{\beta_j}] & [\boldsymbol{\alpha_j}] \end{bmatrix} \text{ and } [U]=\begin{bmatrix} [\mathbf{I}] & [\boldsymbol{\Gamma_1}] & \cdot & \cdot & \cdot & \cdot \\ \cdot & [\mathbf{I}] & [\boldsymbol{\Gamma_2}] & \cdot & \cdot & \cdot \\ \cdot & \cdot & \cdot & \cdot & \cdot & \cdot \\ \cdot & \cdot & \cdot & \cdot & \cdot & \cdot \\ \cdot & \cdot & \cdot & \cdot & \cdot & \cdot \\ \cdot & \cdot & \cdot & \cdot & [\mathbf{I}] & [\boldsymbol{\alpha_{j-1}}] \\ \cdot & \cdot & \cdot & \cdot & \cdot & [\mathbf{I}] \end{bmatrix},$$

where $[I]$ is the matrix of order 7 and $[\alpha_i]$ and $[\Gamma_i]$ are 7x7 matrices which elements determined by the following equation:

$$[\alpha_1]=[A_1],$$

$$[A_1]=[\Gamma_1][C_1],$$

$$[A_J]=[A_{J-1}]-[B_J][\Gamma_{J-1}],\ J=2,3,4,\ldots,J,$$

$$[A_J][\Gamma_J]=[C_J],\ J=2,3,4,\ldots,J-1,$$

$$[L][U][\delta]=[r].$$

If we define $[U][\delta]=[W]$, then equation becomes $[L][W]=[r]$, where

$$[W]=\begin{bmatrix} [W_1] \\ [W_2] \\ \cdot \\ \cdot \\ \cdot \\ [W_{j-1}] \\ [W_j] \end{bmatrix},\ 1\leq j\leq J,$$

and the $[W_j]$ are 7x1 column matrices. The elements W can be solved from

$$[\alpha_1][W_1]=[r_1],$$

$$[\alpha_2][W_j]=\lfloor r_j\rfloor-\lfloor B_j \perp W_j\rfloor,\ 2\leq j\leq J.$$

The step in which Γ_J, $\boldsymbol{\alpha_j}$ and W_j are calculated is usually referred to as the forward sweep. Once the elements of W are found, the solution δ in the so-called backward sweep in which the elements are obtained by the following relations:

$$[\delta_j]=[W_j],$$

$$[\delta_j]=[W_j]-[\Gamma_j][\delta_{j+1}],\ 1\leq j\leq J\text{-}1.$$

These calculations are repeated until some convergence criterion is satisfied and calculations are stopped where $\left|\delta v_0^{(i)}\right|\leq\varepsilon_1$, where ε_1 is a small, prescribed value.

4. Results and discussion

We were able to find a solution to the problem of laminar boundary layer flow in rotating Maxwell fluid that was induced by uniform elastic stretching material. In addition, the CC model is put to use in the study of the characteristics of heat transmission. The primary objective of this section is to present and analyze the impacts that physical parameters have on the solutions, and this will be accomplished through the use of instances. To do this, we depict the temperature and velocity profiles in Figures 3–8.

When λ=0.2, we draw conclusions about the profiles of the non-dimensional x-component of velocity $f'(\eta)$ at various values of the Deborah's number β is shown in Figure 3. Deborah's number contrasts the observation time scale with the fluid relaxation time of memory distortion. When Deborah number is low, the material reacts like a completely viscous fluid and the recovery time is quick. When β increases, the horizontal velocity of the vehicle tends to decrease. A greater value of β implies a more physically significant viscous force, which resists the flow and causes the velocity to drop. When the value of β is increased, we observe that the patterns are skewed in the direction of the border. This suggests that the thickness of the boundary layer decreases as β increases. A substance with a high Deborah number, however, receives a strong like response. When η is increasing and it diminishes beyond the boundary layer, the function $f'(\eta)$ gradually decreases. It is evident that the velocity fluid $f'(\eta)$ and boundary layer thickness decrease as the parameter β, or the parameter associated to fluid relaxation time, increases.

Figure 4 reveals that the behavior of $f'(\eta)$ affects the rotational parameter λ. λ=0 refers to a condition where the frame is not rotating. The ratio of rotation rate to stretching rate rises as λ grows. From a physical perspective, when λ grows, the rotation rate increases more quickly than the stretching rate. Due to rotational effects, the value of f' for bigger values of λ turns negative close to the border.

Figure 5 reveal that the features of Deborah number β on the $g(\eta)$, the sheet is only stretched in the x-direction, therefore flow in the y-direction is only anticipated as a result of the rotating frame, where the magnitude of the velocity field $g(\eta)$, which is proportional to the y-component of velocity, decreases further from the stretching surface. Because of the rotating effect, flow only occurs in the negative y-direction in this case, as indicated by the negative value of $g(\eta)$. The velocity profile $g(\eta)$ as a function of the rotational constant λ is depicts in Figure 6. As can be observed, the rotation parameter helps the flow move in the opposite direction of y. The profile $g(\eta)$ is comparable to the

function -η exp(-η) for lower lambda. However, an oscillating pattern in the profile of $g(\eta)$ is seen for large values of the rotation parameter λ.

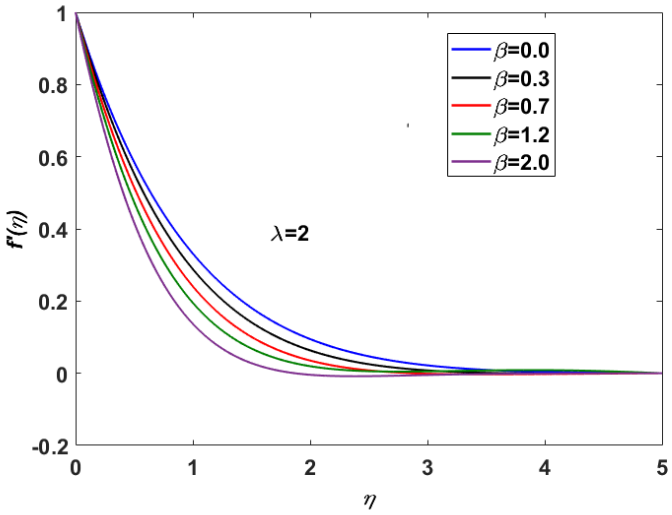

Figure 3. Impact of β on $f'(\eta)$.

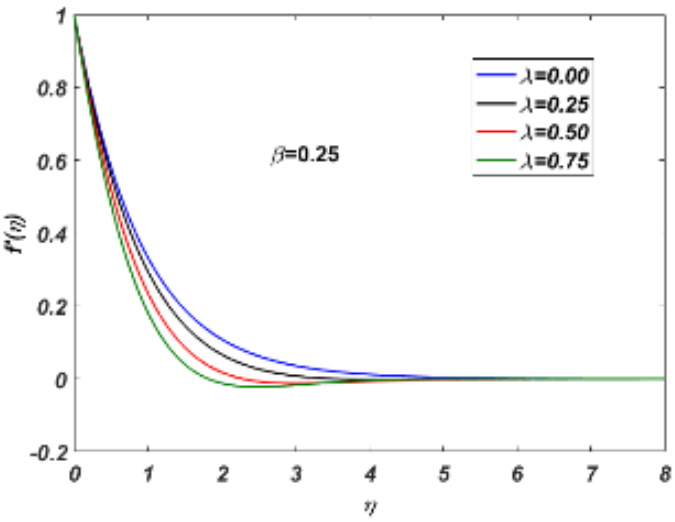

Figure 4. Impact of λ on $f'(\eta)$.

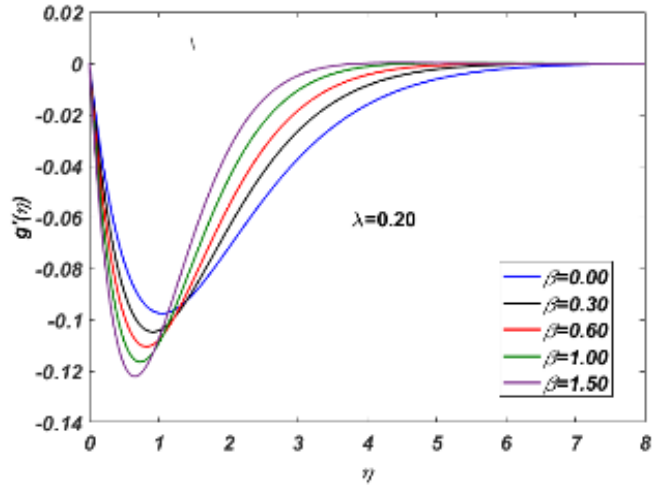

Figure 5. Impact of β on $g(\eta)$.

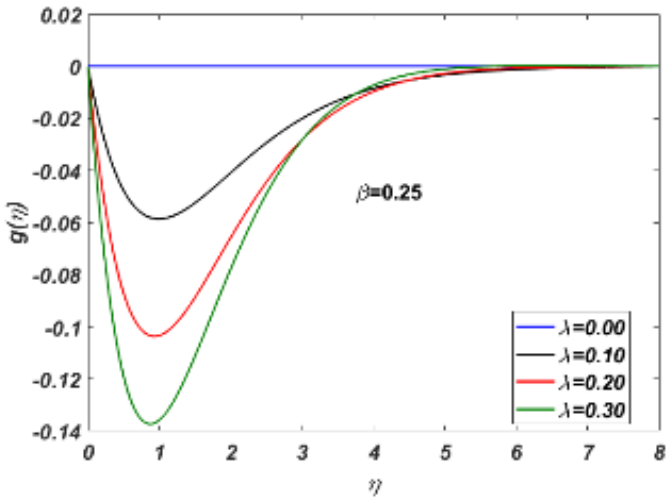

Figure 6. Impact of λ on $g(\eta)$.

Figure 7 shows that the on $\theta(\eta)$ for different values of ε with given values of other factors. In this study, variable thermal conductivity is taken into account, and its expression implies that the parameter ε has a direct relationship to thermal conductivity. A bigger value of ε indicates a larger thermal diffusivity, which results in a thicker temperature penetration depth.

Figure 8 includes the θ curve with non-dimensionality for different thermal relaxation times. The curve tends to move closer to the stretching border when parameter γ is directly proportional to the increase in thermal relaxation time. When a longer thermal relaxation time is taken into account, it suggests that the temperature penetration depth is shortened.

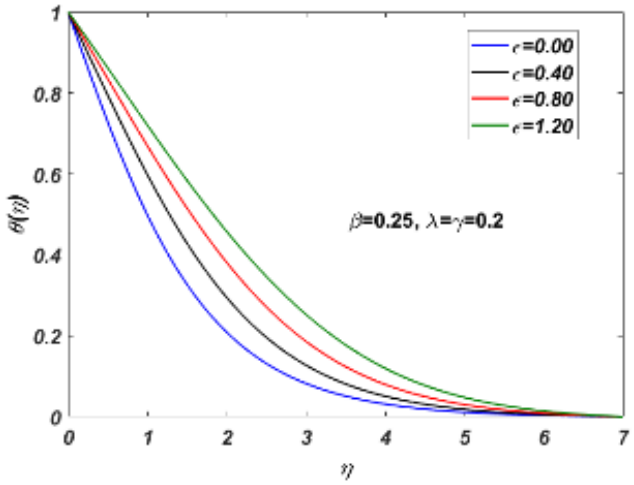

Figure 7. Impact of ϵ on $\theta(\eta)$.

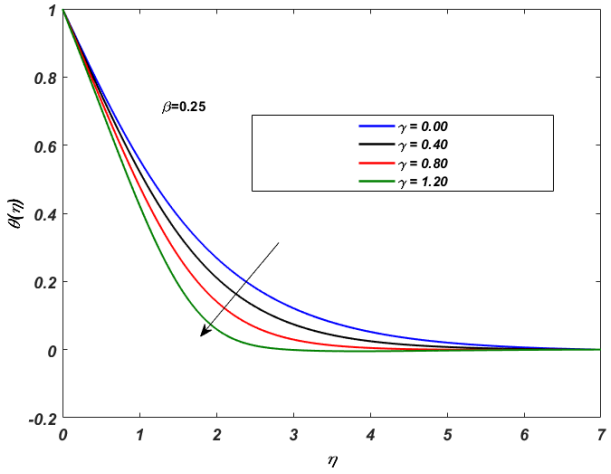

Figure 8. Impact of γ on $\theta(\eta)$.

In order to verify the accuracy of our calculations, we compare the results for $f''(0)$ to those found in the prior literature in the non-rotating frame $\lambda = 0,$ is shown in Table 1. Table 2 contain a numerical summary of the results for the wall velocity gradients $f''(0)$ and $g'(0)$.

Table 1. Code validation test for $f''(0)$ for $\lambda = 0$.

β	Abel et al. [13]	1.000000
0.0	0.999962	1.101903
0.4	1.101850	1.196711
0.8	1.196692	1.285363
1.2	1.285257	1.368758
1.6	1.368641	1.368758
2.0	0.999962	1.000000

Table 2. Numeric data for $f''(0)$ and $g'(0)$ for $\lambda = 0.2$.

β	$-f''(0)$	$-g'(0)$
0.0	1.01091	1.01091
0.4	1.13091	1.13091
0.8	1.19832	1.19832
1.0	1.25312	1.25312
1.2	1.30912	1.30912

5. Conclusions

A numerical investigation of Maxwell thermal fluid flow in a rotating frame with variable thermal conductivity and Cattaneo-Christov heat flux is carried out. A Keller box finite difference-based approach is used to solve nonlinear equations governing self-similar flow. The following summarizes the main features of this work:

- Viscoelastic effects provide flow resistance in both the x and y directions. However, when a larger value of the viscoelastic component β is considered, the temperature θ rises slightly.
- As Pr rises, the wall slope of the temperature rises and becomes closer to zero, which indicates that Pr is vanishing.
- As expected, increasing ϵ increases the thickness of the thermal boundary layer while decreasing the gradient of the wall temperature.
- By putting $\beta = 0$, the current model reduces to the Newtonian fluid condition. The setting $\gamma = 0$ also makes it possible to retrieve the Fourier-law aspect.
- The consideration of rotational effects reduces the thickness of the hydrodynamic boundary layer.

These findings could be extended to include the unsteady dynamics of the incompressible UCM fluids that are caused by body forces.

Conflict of interest

The authors declare no conflict of interest.

References

1. S. H. Han, L. C. Zheng, C. R. Li, X. X. Zhang, Coupled flow and heat transfer in viscoelastic fluid with Cattaneo-Christov heat flux model, *Appl. Math. Lett.*, **38** (2014), 87–93. https://doi.org/10.1016/j.aml.2014.07.013
2. M. Mustafa, Cattaneo-Christov heat flux model for rotating flow and heat transfer of upper-convected Maxwell fluid, *AIP Adv.*, **5** (2015), 047109. https://doi.org/10.1063/1.4917306
3. B. Krishnendu, H. Krishnendu, A. Ahmed, Dual solutions in boundary layer flow of Maxwell fluid over a porous shrinking sheet, *Chinese Phys. B*, **23** (2014), 124701. https://doi.org/10.1088/1674-1056/23/12/124701

4. C. Fetecau, M. Jamil, C. Fetecau, I. Siddique, A note on the second problem of Stokes for Maxwell fluids, *Int. J. Non-Linear Mech.*, **44** (2009), 1085–1090. https://doi.org/10.1016/j.ijnonlinmec.2009.08.003
5. C. Fetecau, M. Athar, C. Fetecau, Unsteady flow of generalized Maxwell fluid with fractional derivative due to a constantly accelerating plate, *Comput. Math. Appl.*, **57** (2009), 596–603. https://doi.org/10.1016/j.camwa.2008.09.052
6. Y. Mahsud, N. A. Shah, D. Vieru, Influence of time-fractional derivatives on the boundary layer flow of Maxwell fluids, *Chinese J. Phys.*, **55** (2017), 1340–1351. https://doi.org/10.1016/j.cjph.2017.07.006
7. I. Khan, N. A. Shah, L. C. C. Dennis, A scientific report on heat transfer analysis in mixed convection flow of Maxwell fluid over an oscillating vertical plate, *Sci. Rep.*, **7** (2017), 40147. https://doi.org/10.1038/srep40147
8. S. K. Nandy, Unsteady flow of Maxwell fluid in the presence of nanoparticles toward a permeable shrinking surface with Navier slip, *J. Taiwan Inst. Chem. Eng.*, **52** (2015) 22–30. https://doi.org/10.1016/j.jtice.2015.01.025
9. W. Na, N. A. Shah, I. Tlili, I. Siddique, Maxwell fluid flow between vertical plates with damped shear and thermal flux: free convection, *Chinese J. Phys.*, **65** (2020), 367–376. https://doi.org/10.1016/j.cjph.2020.03.005
10. L. M. Cao, X. H. Si, L. C. Zheng, Convection of Maxwell fluid over stretching porous surface with heat source/sink in presence of nanoparticles: Lie group analysis, *Appl. Math. Mech.*, **37** (2016), 433–442. https://doi.org/10.1007/s10483-016-2052-9
11. M. E. Karim, M. A. Samad, Effect of Brownian diffusion on squeezing elastico-viscous nanofluid flow with Cattaneo-Christov heat flux model in a channel with double slip effect, *Appl. Math.*, **11** (2020), 277–291. https://doi.org/10.4236/am.2020.114021
12. S. Shateyi, S. S. Motsa, Thermal radiation effects on heat and mass transfer over an unsteady stretching surface, *Math. Probl. Eng.*, **2009** (2009), 1–13. https://doi.org/10.1155/2009/965603
13. M. S. Abel, J. V. Tawade, J. N. Shinde, The effects of MHD flow and heat transfer for the UCM fluid over a stretching surface in presence of thermal radiation, *Adv. Math. Phys.*, **2012** (2012), 1–21. https://doi.org/10.1155/2012/702681
14. C. I. Christov, On frame indifferent formulation of the Maxwell-Cattaneo model of finite-speed heat conduction, *Mech. Research Commun.*, **36** (2009), 481–486. https://doi.org/10.1016/j.mechrescom.2008.11.003
15. B. Straughan, Thermal convection with the Cattaneo-Christov model, *Int. J. Heat Mass Transfer*, **53** (2010), 95–98. https://doi.org/10.1016/j.ijheatmasstransfer.2009.10.001
16. V. Tibullo, V. Zampoli, A uniqueness result for the Cattaneo-Christov heat conduction model applied to incompressible fluids, *Mech. Research Commun.*, **38** (2011), 77–79. https://doi.org/10.1016/j.mechrescom.2010.10.008

17. S. A. M. Haddad, Thermal instability in Brinkman porous media with Cattaneo-Christov heat flux, *Int. J. Heat Mass Transfer*, **68** (2014), 659–668. https://doi.org/10.1016/j.ijheatmasstransfer.2013.09.039
18. R. M. Khan, N. Imran, Z. Mehmood, M. Sohail, A Petrov-Galerkin finite element approach for the unsteady boundary layer upper-convected rotating Maxwell fluid flow and heat transfer analysis, *Waves Random Complex Media*, **2022** (2022), 1–18. https://doi.org/10.1080/17455030.2022.2055201
19. S. Bilal, A. H. Majeed, R. Mahmood, I. Khan, A. H. Seikh, E. S. M. Sherif, Heat and mass transfer in hydromagnetic second-grade fluid past a porous inclined cylinder under the effects of thermal dissipation, diffusion and radiative heat flux, *Energies*, **13** (2020), 1–17. https://doi.org/10.3390/en13010278
20. A. H. Majeed, S. Bilal, R. Mahmood, M. Y. Malik, Heat transfer analysis of viscous fluid flow between two coaxially rotated disks embedded in permeable media by capitalizing non-Fourier heat flux model, *Phys. A*, **540** (2020), 1231182 https://doi.org/10.1016/j.physa.2019.123182
21. S. Bilal, A. Tassaddiq, A. H. Majeed, K. S. Nisar, F. Ali, M. Y. Malik, Computational and physical examination about the aspects of fluid flow between two coaxially rotated disks by capitalizing non-Fourier heat flux theory: finite difference approach, *Front. Phys.*, **7** (2019), 209. https://doi.org/10.3389/fphy.2019.00209

AIMS Press